Hindawi Publishing Corporation
Journal of Nanomaterials
Volume 2011, Article ID 510237, 7 pages
doi:10.1155/2011/510237

Research Article

Fabrication and Optical Property of Periodic $Sn_{1-x}Ti_xO_2$ Nanostructures Patterned by the Polystyrene Microsphere Templates

Shutian Chen, Zhengcao Li, and Zhengjun Zhang

Advanced Materials Laboratory, Department of Materials Science and Engineering, Tsinghua University, Beijing 100084, China

Correspondence should be addressed to Zhengcao Li, zcli@tsinghua.edu.cn

Received 28 June 2011; Revised 31 August 2011; Accepted 13 September 2011

Academic Editor: Yanqiu Zhu

Regular arrays of $Sn_{1-x}Ti_xO_2$ nanostructures were fabricated by glancing angle sputter deposition onto self-assembled close-packed arrays of 200 nm diameter, 500 nm diameter, and 1 μm diameter polystyrene microspheres, respectively. The morphology of the nanostructures could be modulated by the variation of the sputtering power of Ti target and the size of polystyrene microspheres templates. Accordingly, the performance of reflection which was dependent on the morphology of nanostructures could be tuned by optimizing the parameters. The anisotropic morphology of nanoflakes achieved by adjusting the sputtering power of Ti target could generate the anisotropism of reflectance. With the increase of the PS sphere size, the anisotropism of nanostructures weakened; however, they exhibited excellent antireflection effects by creating a smaller gradient of refractive index.

1. Introduction

Much attention has been attracted to the design of nanoscale semiconductor oxide materials with controlled morphology and novel morphology-dependent properties. Recently, subwavelength grating (SWG) structures with a moth-eye profile have aroused the interest of researchers [1–3]. The surface of the moth eye is covered by highly packed protuberances, which reduce the reflection and thus improve the visual efficiency. The operation of SWG structures is similar to the moth eye. From the viewpoint of the effective medium theory, the nanostructures can be considered as a homogeneous medium with a graded refractive index which varies gradually from 1.0 (air) to that of the bulk material [4]. Therefore, the reflection can be reduced significantly by SWG structures with tapered features. The antireflection structures exhibit great potentials in the applications of solar cells, LEDs, photodetectors, transparent glasses, and so on [5–8].

Tin dioxide (SnO_2) is an n-type semiconductor with a wide band gap (Eg = 3.6 eV at 300 K) that is well known for its promising applications in gas sensing [9], lithium-ion batteries [10], photocatalysis [11], and dye-sensitized solar cells (DSCs) [12]. Similar to other highly transparent semiconductors, SnO_2 is also expected to be a competitive candidate for optical devices [13–15]. Due to the isostructure (rutile type) and close lattice parameters of TiO_2 and SnO_2, the metal cations can be replaced by each other in a wide concentration region. Hence, Ti is an appealing alternative of doping, compared with other elements whose contents are restricted to a low level since the emergence of the second phase [16]. In our study, we have successfully yielded periodic arrays of $Sn_{1-x}Ti_xO_2$ nanostructures by glancing angle sputter deposition onto self-assembled close-packed arrays of polystyrene spheres. The morphology of the $Sn_{1-x}Ti_xO_2$ nanostructures could be controlled by changing the sputtering power of Ti target and the size of polystyrene microspheres templates. Accordingly, their optical properties could be tuned by adjusting the parameters. Such unique structures with modulated morphology and designed optical performance are promising to be applied in optical devices.

2. Experimental Details

The $Sn_{1-x}Ti_xO_2$ nanostructures were prepared in an ultra-high vacuum magnetron sputter deposition system on Si

(001) substrates that were patterned with 200 nm diameter, 500 nm diameter, and 1 μm diameter hexagonal close-packed polystyrene microspheres, respectively. $Sn_{1-x}Ti_xO_2$ depositions were carried out using a 6 cm diameter Ti target (99.99% pure) and a 6 cm diameter SnO_2 target (99.9% pure) mounted at an angle of 120° with respect to each other, and with the Ti target back to the substrate. The deposition angle α (the angle between the trajectory of the incident vapor flux and the substrate normal), which was controlled by the substrate position with respect to the Ti target, was selected to be 85°. Sputtering was carried out at 0.15 Pa which was held constant during all depositions in 99.999% pure Ar. No external substrate heating was applied. Power-regulated DC and RF power supplies were used to provide the discharge currents of 0.20 A, 0.25 A, 0.30 A, and 0.35 A, respectively, at 340 V for Ti, and a radio frequency current of 130 mA at 500 V for SnO_2. The $Sn_{1-x}Ti_xO_2$ nanostructures were obtained with the simultaneous deposition from the sputtering sources of Ti and SnO_2 onto a stationary substrate. The morphology of all samples was examined by a scanning electron microscope (SEM), with their structure identified by X-ray diffraction (XRD) analysis, and the reflectance was measured by a spectrophotometer.

3. Results and Discussion

The $Sn_{1-x}Ti_xO_2$ nanostructures were prepared on Si (001) substrates that were patterned with 200 nm diameter, 500 nm diameter, and 1 μm diameter hexagonal close-packed polystyrene microspheres, respectively. In the depositions, the power of RF sputtering was fixed while the power of DC sputtering was regulated at the discharge currents = 0.20 A, 0.25 A, 0.30 A, and 0.35 A, respectively, for each size of PS microsphere templates. Correspondingly the prepared samples were named 1#, 2#, 3#, and 4#. The structures of films were identified by X-ray diffraction (XRD), indicating the amorphous state in all the samples.

The morphology and optical properties of the $Sn_{1-x}Ti_xO_2$ nanostructures with different PS sphere sizes were studied, respectively. First, Figure 1 shows typical SEM micrographs of 1# and 2# grown on 200 nm, 500 nm, and 1 μm PS microspheres. Arrays of well-separated $Sn_{1-x}Ti_xO_2$ nanostructures were produced. The regular hexagonal arrays replicate the close-packed pattern of the polystyrene spheres, attributed to the limited adatom surface diffusion and atomic shadowing effects in the process of GLAD. The films deposited on 200 nm diameter PS spheres exhibit anisotropic morphology of melon seed-shape nanoflakes, as shown in Figures 1(a) and 1(b). The formation of nanoflakes can be explained by the mechanism of GLAD. As GLAD is a physical vapor deposition process in which the incident flux impinges the substrate from an oblique angle, causing atomic shadowing and the resulting highly porous nanostructures [17–19], the morphology of nanostructures is closely related to the direction of the incident flux. With the incident flux from lateral SnO_2 target, the direction of the growth front is changed from straight up to lateral growth, leading to an increase of the growth rate in the direction parallel to the SnO_2 flux and a decrease in the perpendicular direction [20]. As a result, the nanostructures are deformed by the anisotropic lateral growth and exhibit the anisotropic morphology of melon seed-shaped nanoflakes. From Figures 1(a) and 1(b), the height of nanostructures is 400 nm approximately with the diameter of PS spheres deducted, which is comparable with respect to the scale of PS spheres. When the size of PS microspheres is increased to 500 nm, it indicates that the films still exhibit the anisotropy to some extent, as shown in Figures 1(c) and 1(d), though less distinctly compared with that deposited on 200 nm diameter PS spheres. As the size of the template is further increased, the nanostructures become "spheric shells" covering the polystyrene microspheres, which is shown in Figures 1(e) and 1(f).

Comparing the films with different PS sphere sizes, it can be concluded that the anisotropy of morphology degenerates gradually with the increase of the template size. When grown on 200 nm diameter PS microspheres, the anisotropic nanoflakes are yielded in the film 1# and 2#. With the size of PS microspheres increased, the nanostructures degenerate to asymmetric "spheric shells" gradually. This result matches well with the growing mechanism of the nanoflakes. For the deposition layer is relatively thin, the anisotropic lateral growth is overwhelmed by the effect of templates gradually with the increase of the template size, causing the degeneration from nanoflakes to asymmetric "spheric shells".

The morphology of film 3# and 4# with various PS sphere sizes is shown in Figure 2. As discussed before, the morphology of nanostructures is influenced by the anisotropic lateral growth deriving from the incident flux. Therefore, with the increased sputtering rate of Ti target, the effect of lateral SnO_2 flux was overweighed by the Ti flux, resulting in the transition of the nanostructures from nanoflakes to nanopillars, as shown in Figures 2(a) and 2(b). Similarly, the film 3# and 4# turn to short nanopillars when deposited on 500 nm diameter PS spheres, and symmetric "spheric shells" on 1 μm diameter PS spheres, which is indicated in Figures 2(c)–2(f). Besides, there is an interesting phenomenon worth noticing. Both as nanopillars, it is clear that the surface of film 4# is coarser than film 3# with the increase of the sputtering power, as shown in Figures 2(a) and 2(b). With the size of PS microspheres increased to 500 nm, there are subrods protruding out from the tips of nanopillars in film 4#; when the size of the template is increased to 1 μm, more subrods are formed both in the film 3# and 4#, as shown in Figures 2(c)–2(f).

The effect of templates to the subrods is noteworthy. The nucleation of subrods is caused by surface mounds that capture, due to atomic shadowing, a larger fraction of the deposition flux than the surrounding surface. With the elevated sputtering power, the adatom mobility is limited with respect to the high-speed deposition, which leads to kinetic roughening [21, 22]. Once one or multiple surface mounds have developed on a single nanostructure, atomic shadowing favors the growth of the mounds, leading to the formation of subrods on the top ultimately. For the films deposited on 200 nm diameter PS microspheres, the roughening of the surface of nanostructures is observed, when the sputtering current is lifted to 0.35 A. However, there

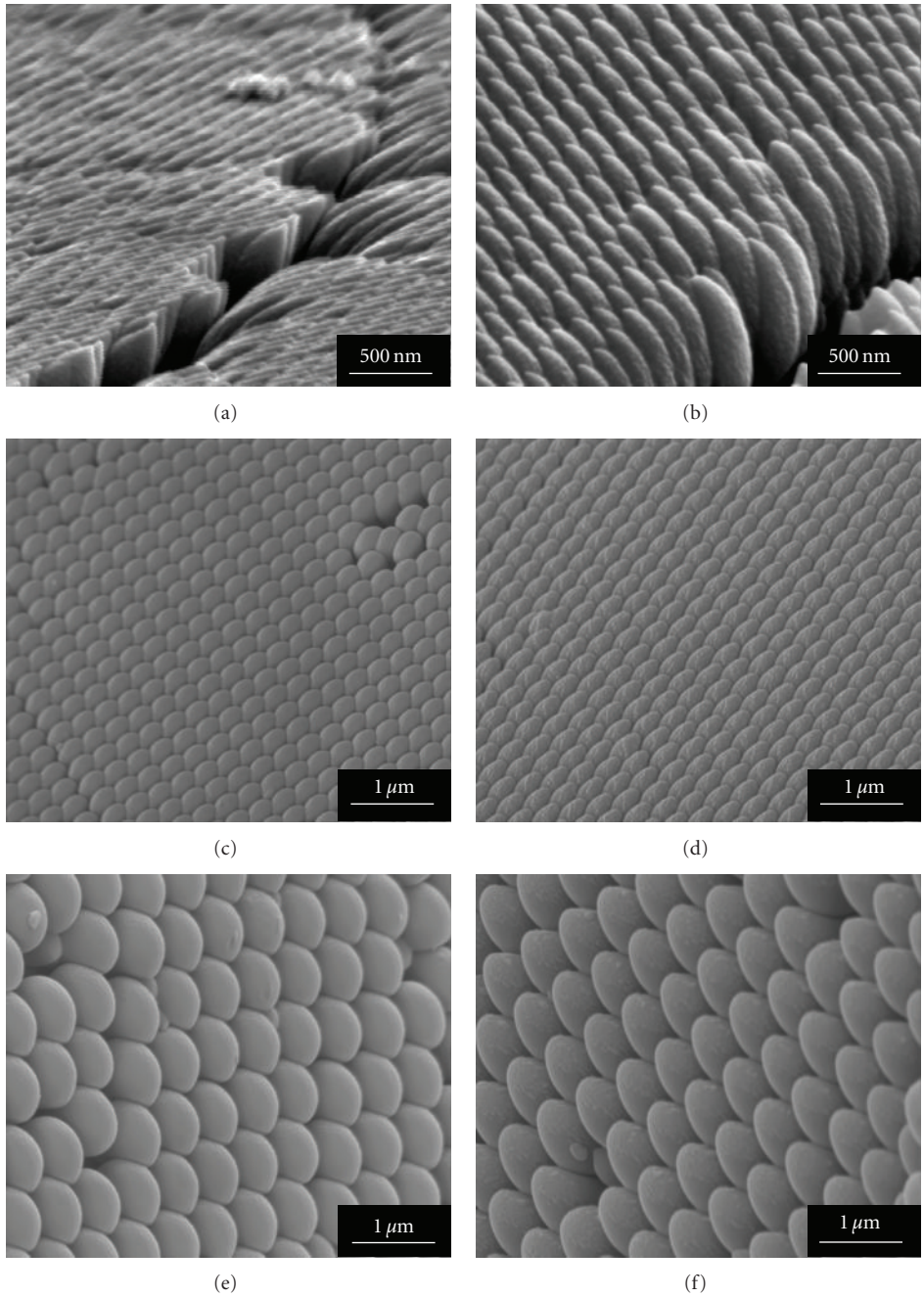

FIGURE 1: Scanning electron microscopic images of $Sn_{1-x}Ti_xO_2$ films deposited on 200 nm, 500 nm, and 1 μm PS spheres at I (the discharge currents) of Ti target 0.20 A and 0.25 A (a) film 1# at $I = 0.20$ A on 200 nm PS spheres; (b) film 2# at $I = 0.25$ A on 200 nm PS spheres; (c) film 1# at $I = 0.20$ A on 500 nm PS spheres; (d) film 2# at $I = 0.25$ A on 500 nm PS spheres; (e) film 1# at $I = 0.20$ A on 1 μm PS spheres; (f) film 2# at $I = 0.25$ A on 1 μm PS spheres.

are not any subrods existing. The subrods begin appearing in the film 4# with a PS sphere size of 500 nm, and increase significantly in the film 3# and 4# with a PS sphere size of 1 μm. It is in agreement with the preceding discussion. Because the nanostructures replicate the close-packed array of the initial surface pattern, the size of templates is required to be larger than the surface mound separation for the nucleation of subrods. Therefore, the subrods cannot form when grown on 200 nm diameter PS microspheres. Conversely, the probability of subrods is expected to increase substantially with the increase of the template size, ascribed to more surface mounds.

Because the optical properties of films are dependent on the morphology of nanostructures, which is quite related with the size of PS microspheres templates, the comparison of the reflectance between the films with different PS sphere

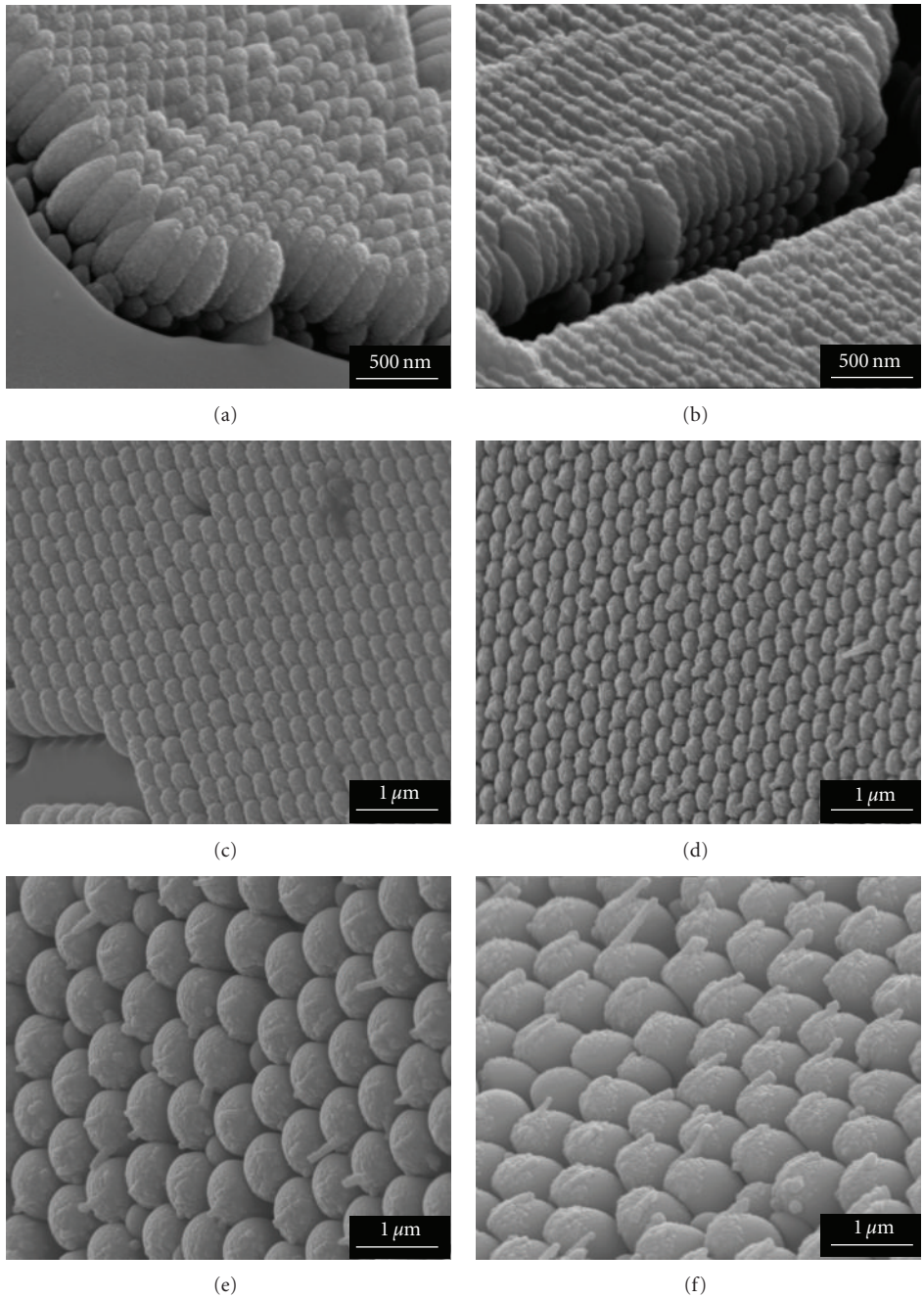

Figure 2: Scanning electron microscopic images of $Sn_{1-x}Ti_xO_2$ films deposited on 200 nm, 500 nm and 1 μm PS spheres at I (the discharge currents) of Ti target 0.30 A and 0.35 A (a) film 3# at $I = 0.30$ A on 200 nm PS spheres; (b) film 4# at $I = 0.35$ A on 200 nm PS spheres; (c) film 3# at $I = 0.30$ A on 500 nm PS spheres; (d) film 4# at $I = 0.35$ A on 500 nm PS spheres; (e) film 3# at $I = 0.30$ A on 1 μm PS spheres; (f) film 4# at $I = 0.35$ A on 1 μm PS spheres.

sizes was conducted. The reflectance of films was measured by a spectrophotometer. Figure 3(a) shows the directions of incident light. The reflectance in the direction parallel to the surface of the nanoflakes is marked as $R_{//}$ while the reflectance in the other direction is marked as $R_{\perp}$. The definition of $R_{//}$ and $R_{\perp}$ is consistent for the films with various PS sphere sizes. Figures 3(b) and 3(c) provide the $R_{//}$ and $R_{\perp}$ of film 1# and 2# in the spectral range 300–750 nm. It is evident that for the film 1# and 2# deposited on 200 nm diameter PS spheres, $R_{//}$ is considerably lower than $R_{\perp}$. However, the anisotropy of reflectance for the films with a PS sphere size of 500 nm lowers significantly; the reflectance for the films with a PS sphere size of 1 μm is all fairly low in the whole spectral region, and no apparent anisotropy is observed. This result is consistent with the trend of the anisotropy of the morphology.

Figures 4(a) and 4(b) provide the $R_{//}$ and $R_{\perp}$ of film 3# and 4# with various PS sphere sizes. It indicates that,

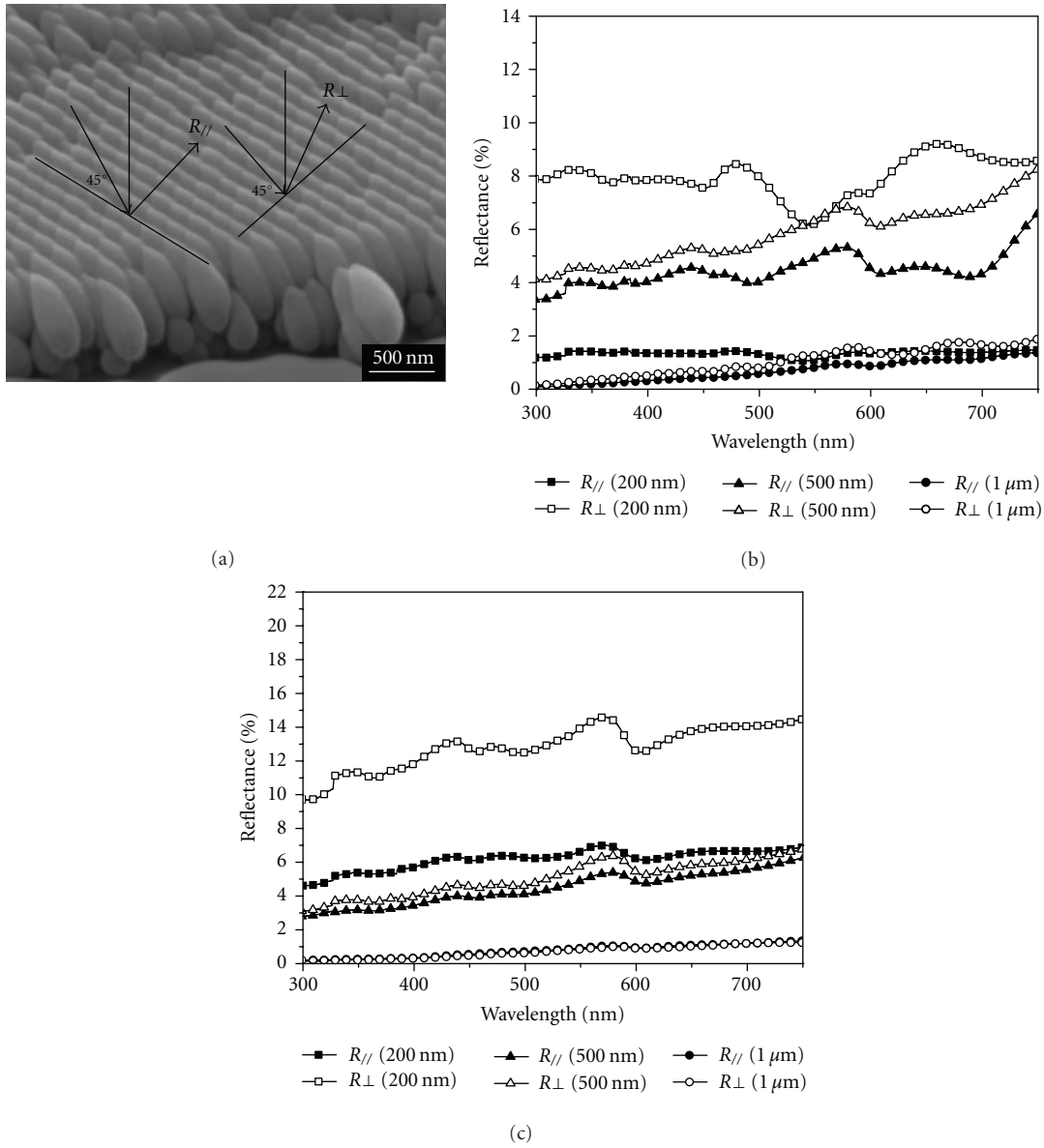

Figure 3: The sketch of the incident and reflected light, with the reflectance in two directions marked as $R_{//}$ and $R_{\perp}$, respectively (a), and the $R_{//}$ and $R_{\perp}$ of film 1# (b) and 2# (c) with various PS sphere sizes at the wavelength range of 300–750 nm.

compared with film 1# and 2#, the reflectance of these films is almost isotropic except for the film 4# deposited on 500 nm PS spheres, probably owing to the subrods on the surface. However, the subrods-induced anisotropy is not observed for the film 3# and 4# with a PS sphere size of 1 μm, though there are even more subrods obtained, which is likely because the reflectance is too low to be differentiated. On the other hand, it can be concluded that the reflectance of films shows a decrease trend with the increase of the PS sphere size from Figures 3 and 4.

The result of reflectance can be explained by the model of two-dimensional submicrometer antireflection coatings. Since the application of conventional single-layer antireflection coatings is limited at a single wavelength only, the gradient-refractive index antireflection coating inspired biologically by moth eyes becomes a desirable alternative. The "moth eye" antireflection surface consisting of submicron structure arrays, with refractive index varying monotonically from the air to the substrate along its thickness, can be thought of as a set of multilayers with minimal difference in the refractive index according to effective medium theory and effectively suppress the specular reflectance at the interface of the two media [23, 24]. Therefore, periodic nanostructures which could lead to an effective refractive index gradient were designed to diminish the reflection [25–27]. The nanostructures we prepared, with tapered profile, can be approximately equivalent to a gradient-refractive index submicrometer coating. The effect of "moth eye" antireflection surface depends on the height and profile of the submicron structures. Accordingly, the reflectance can be tuned by the sputtering parameters and the size of PS microsphere templates, which have a great influence

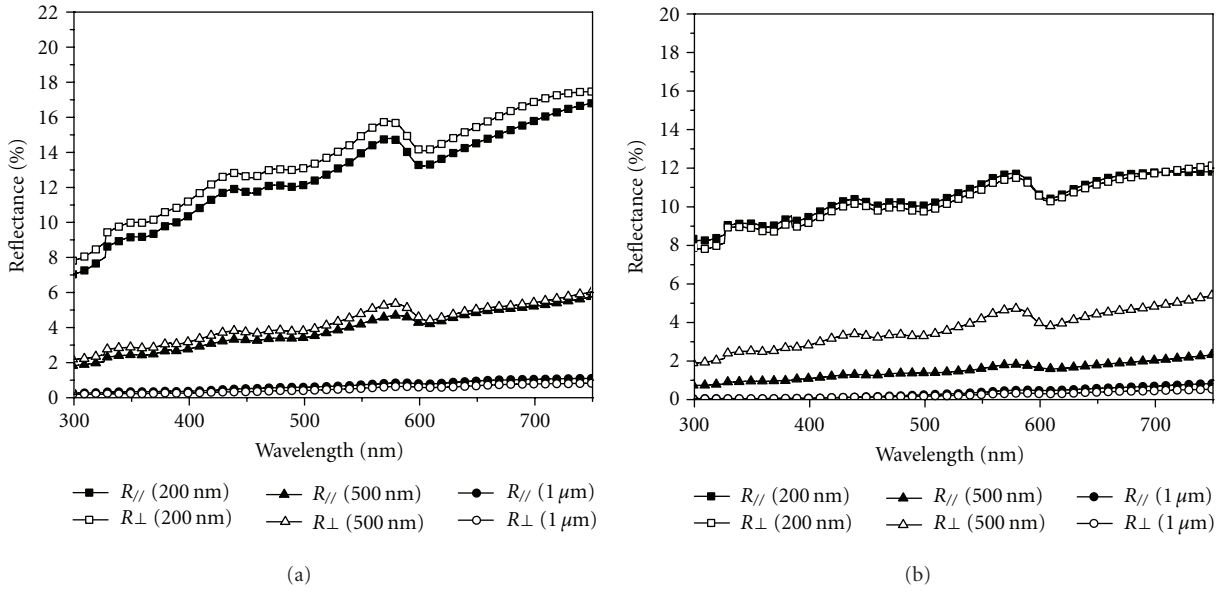

FIGURE 4: The $R_{//}$ and $R_{\perp}$ of film 3# (a) and 4# (b) with various PS sphere sizes at the wavelength range of 300–750 nm.

on the height and shape of periodic structures. On one hand, the sputtering parameter is correlated with the interaction of the incident flux and impacts the morphology of nanostructures. As the anisotropy of the morphology plays a crucial role in the anisotropy of reflectance, the anisotropy of reflectance weakens with the increase of sputtering power of Ti target. On the other hand, the periodicity of nanostructure arrays is also a critical factor. The nanostructure array with a smaller periodicity displays apparent anisotropy of reflectance, while a larger periodicity is not beneficial for it, resulting from the effect of templates on the anisotropic lateral growth. However, the films grown on 1 μm diameter PS spheres render a better antireflection effect in comparison to that grown on 200 nm diameter, and 500 nm diameter PS spheres. Because the increase of the height of nanostructures generates smaller effective-index gradient, the reflection is progressively reduced with increased height and the film deposited on 1 μm PS spheres demonstrates superior antireflection performance [28, 29].

In summary, the preparation method of glancing angle sputter deposition we proposed can accomplish the adjustment to the morphology of nanostructures, and ultimately the tuning to the optical property. Porous and textured surfaces with a graded refractive index can be generated by obliqueness of the incident flux. It is worth to mention its advantages over the top-down method. As the most popular technique to fabricate antireflection films, the top down method, including wet or dry etching, is preferred as the precise control over the nanostructures. However, this method has some limitations: it is difficult to achieve smaller diameter or period and too costly for the multiple complicated and time-consuming process steps. Compared to the top down method, the glancing angle sputter deposition shows great potential in optical device applications.

4. Conclusions

We have demonstrated closely packed and morphology-controlled $Sn_{1-x}Ti_xO_2$ nanostructures on patterned Si substrates by glancing angle sputter deposition, indicating unique optical properties in the visible region. The shape of the $Sn_{1-x}Ti_xO_2$ nanostructures could be controlled by adjusting the sputtering power of Ti target and the periodicity of nanostructure arrays, which was dominated by the size of PS sphere templates. The anisotropic morphology of nanoflakes achieved by adjusting the sputtering power of Ti target could generate the anisotropism of reflectance, a phenomenon that was of interest for applications. A smaller periodicity was preferable to the anisotropism of morphology and reflectance, while a larger periodicity was not beneficial for it. However, they provided substantially reduced reflectance as the smaller effective-index gradient. These nanostructures with controlled morphology and optical properties are expected to open up application areas as optical devices.

Acknowledgments

The authors are grateful to the financial support by the National Basic Research Program of China (973 program, 2010CB731600) and the National Natural Science Foundation of China (51072094 and 61076003).

References

[1] S. A. Boden and D. M. Bagnall, "Tunable reflection minima of nanostructured antireflective surfaces," *Applied Physics Letters*, vol. 93, no. 13, Article ID 133108, 2008.

[2] Z. Yu, H. Gao, W. Wu, H. Ge, and S. Y. Chou, "Fabrication of large area subwavelength antireflection structures on Si using trilayer resist nanoimprint lithography and liftoff," *Journal of Vacuum Science and Technology B*, vol. 21, no. 6, pp. 2874–2877, 2003.

[3] K. Kintaka, J. Nishii, A. Mizutani, H. Kikuta, and H. Nakano, "Antireflection microstructures fabricated upon fluorine-doped SiO_2 films," *Optics Letters*, vol. 26, no. 21, pp. 1642–1644, 2001.

[4] J. Huang, X. Wang, and Z. L. Wang, "Bio-inspired fabrication of antireflection nanostructures by replicating fly eyes," *Nanotechnology*, vol. 19, no. 2, Article ID 025602, 2008.

[5] P. Lalanne and G. M. Morris, "Antireflection behavior of silicon subwavelength periodic structures for visible light," *Nanotechnology*, vol. 8, no. 2, pp. 53–56, 1997.

[6] Y. F. Huang, S. Chattopadhyay, Y. J. Jen et al., "Improved broadband and quasi-omnidirectional anti-reflection properties with biomimetic silicon nanostructures," *Nature Nanotechnology*, vol. 2, no. 12, pp. 770–774, 2007.

[7] Y. Peichen, C. H. Chang, C. H. Chiu et al., "Efficiency enhancement of gaas photovoltaics employing antireflective indium tin oxide nanocolumns," *Advanced Materials*, vol. 21, no. 16, pp. 1618–1621, 2009.

[8] T. Lohmüller, M. Helgert, M. Sundermann, R. Brunner, and J. P. Spatz, "Biomimetic interfaces for high-performance optics in the deep-UV light range," *Nano Letters*, vol. 8, no. 5, pp. 1429–1433, 2008.

[9] K. M. Li, Y. J. Li, M. Y. Lu, C. I. Kuo, and L. J. Chen, "Direct conversion of single-Layer SnO nanoplates to multi-layer SnO_2 nanoplates with enhanced ethanol sensing properties," *Advanced Functional Materials*, vol. 19, no. 15, pp. 2453–2456, 2009.

[10] H. X. Zhang, C. Feng, Y. C. Zhai, K. L. Jiang, Q. Q. Li, and S. S. Fan, "Cross-stacked carbon nanotube sheets uniformly loaded with SnO_2 nanoparticles: a novel binder-free and high-capacity anode material for lithium-ion batteries," *Advanced Materials*, vol. 21, no. 22, pp. 2299–2304, 2009.

[11] M. Niu, F. Huang, L. Cui, P. Huang, Y. Yu, and Y. Wang, "Hydrothermal synthesis, structural characteristics, and enhanced photocatalysis of SnO_2/α-Fe_2O_3 semiconductor nanoheterostructures," *ACS Nano*, vol. 4, no. 2, pp. 681–688, 2010.

[12] S. Gubbala, V. Chakrapani, V. Kumar, and M. K. Sunkara, "Band-edge engineered hybrid structures for dye-sensitized solar cells based on SnO_2 nanowires," *Advanced Functional Materials*, vol. 18, no. 16, pp. 2411–2418, 2008.

[13] Z. Weichang, L. Ruibin, W. Qiang et al., "Bound exciton and optical properties of SnO_2 One-Dimensional nanostructures," *Journal of Physical Chemistry C*, vol. 113, no. 5, pp. 1719–1726, 2009.

[14] J. H. He, T. H. Wu, C. L. Hsin et al., "Beaklike SnO_2 nanorods with strong photoluminescent and field-emission properties," *Small*, vol. 2, no. 1, pp. 116–120, 2006.

[15] S. Mathur and S. Barth, "Molecule-based chemical vapor growth of aligned SnO_2 nanowires and branched SnO_2/V_2O_5 heterostructures," *Small*, vol. 3, no. 12, pp. 2070–2075, 2007.

[16] T. Hirata, K. Ishioka, M. Kitajima, and H. Doi, "Concentration dependence of optical phonons in the TiO_2-SnO_2 system," *Physical Review B*, vol. 53, no. 13, pp. 8442–8448, 1996.

[17] Q. Zhou, Z. Li, Y. Yang, and Z. Zhang, "Arrays of aligned, single crystalline silver nanorods for trace amount detection," *Journal of Physics D: Applied Physics*, vol. 41, no. 15, Article ID 152007, 2008.

[18] Q. Zhou, Y. Yang, J. Ni, Z. Li, and Z. Zhang, "Rapid recognition of isomers of monochlorobiphenyls at trace levels by surface-enhanced Raman scattering using Ag nanorods as a substrate," *Nano Research*, vol. 3, no. 6, pp. 423–428, 2010.

[19] Q. Zhou, Z. Li, J. Ni, and Z. Zhang, "A simple model to describe the rule of glancing angle deposition," *Materials Transactions*, vol. 52, no. 3, pp. 469–473, 2011.

[20] S. V. Kesapragada and D. Gall, "Anisotropic broadening of Cu nanorods during glancing angle deposition," *Applied Physics Letters*, vol. 89, no. 20, Article ID 203121, 2006.

[21] C. M. Zhou and D. Gall, "Branched Ta nanocolumns grown by glancing angle deposition," *Applied Physics Letters*, vol. 88, no. 20, Article ID 203117, 2006.

[22] C. M. Zhou and D. Gall, "The structure of Ta nanopillars grown by glancing angle deposition," *Thin Solid Films*, vol. 515, no. 3, pp. 1223–1227, 2006.

[23] H. Sankur and W. H. Southwell, "Broadband gradient-index antireflection coating for ZnSe," *Applied Optics*, vol. 23, no. 16, pp. 2770–2773, 1984.

[24] S. Chattopadhyay, Y. F. Huang, Y. J. Jen, A. Ganguly, K. H. Chen, and L. C. Chen, "Anti-reflecting and photonic nanostructures," *Materials Science and Engineering R*, vol. 69, no. 1–3, pp. 1–35, 2010.

[25] M. A. Ray, N. Shewmon, S. Bhawalkar, L. Jia, Y. Yang, and E. S. Daniels, "Submicrometer surface patterning using interfacial colloidal particle self-assembly," *Langmuir*, vol. 25, no. 13, pp. 7265–7270, 2009.

[26] A. Čampa, O. Isabella, R. van Erven et al., "Optimal design of periodic surface texture for thin-film a-Si:H solar cells," *Progress in Photovoltaics: Research and Applications*, vol. 18, no. 3, pp. 160–167, 2010.

[27] Y. M. Song, E. S. Choi, J. S. Yu, and Y. T. Lee, "Light-extraction enhancement of red AlGaInP light-emitting diodes with antireflective subwavelength structures," *Optics Express*, vol. 17, no. 23, pp. 20991–20997, 2009.

[28] Y. M. Song, S. Y. Bae, J. S. Yu, and Y. T. Lee, "Closely packed and aspect-ratio-controlled antireflection subwavelength gratings on GaAs using a lenslike shape transfer," *Optics Letters*, vol. 34, no. 11, pp. 1702–1704, 2009.

[29] Y. M. Song and Y. T. Lee, "Investigation of geometrical effects of antireflective subwavelength grating structures for optical device applications," *Optical and Quantum Electronics*, vol. 41, no. 10, pp. 771–777, 2009.